Soft Matter

Accepted Manuscript

This article can be cited before page numbers have been issued, to do this please use: V. Calabrese, M. A. da Silva, J. Schmitt, J. Munoz-Garcia, V. Gabrielli, J. L. Scott, J. Angulo, Y. Z. Khimyak and K. J. Edler, *Soft Matter*, 2018, DOI: 10.1039/C8SM00752G.

ROYAL SOCIETY OF CHEMISTRY

rsc.li/soft-matter-journal

View Article Online
DOI: 10.1039/C8SM00752G

Journal Name

ARTICLE

Surfactant controlled zwitterionic cellulose nanofibril dispersions

Vincenzo Calabrese[a] , Marcelo A. da Silva,[a] Julien Schmitt,[a] Juan C. Muñoz-Garcia,[b] Valeria Gabrielli,[b] Janet L. Scott,[a,c] Jesus Angulo,[b] Yaroslav Z. Khimyak,[b] Karen J. Edler*[a]

Received 00th January 20xx,
Accepted 00th January 20xx

DOI: 10.1039/x0xx00000x

www.rsc.org/

Zwitterionic cellulose nanofibrils (ZCNF) with isoelectric point of 3.4 were obtained by grafting glycidyltrimethylammonium chloride onto TEMPO/NaBr/NaOCl-oxidised cellulose nanofibrils. ZCNF aqueous dispersions were characterized via transmission electron microscopy, rheology and small angle neutron scattering, revealing a fibril-bundle structure with pronounced aggregation at pH 7. Surfactants were successfully employed to tune the stability of the ZCNF dispersions. Upon addition of the anionic surfactant, sodium dodecyl sulfate, the ZCNF dispersion shows individualized fibrils due to electrostatic stabilization. On the contrary, upon addition of the cationic species dodecyltrimethylammonium bromide, the dispersion undergoes charge neutralization, leading to more pronounced flocculation.

Introduction

Zwitterionic polymers are a class of polyampholytes, containing anionic and cationic groups with neutral net charge at a specific pH.[1] In the last decade this class of compounds has received attention for metal binding,[2] antifouling[3–5] and antimicrobial[6] properties and their application in drug delivery[7] and encapsulation.[8,9]

The self-assembly and the stabilization of zwitterionic moieties depends on pH, ionic strength and temperature;[10] ideal features for the development of responsive materials.[2,11] At the isoelectric point (IP), polyampholyte polymers (*e.g.* proteins) show charge symmetry between the negatively and positively charged moieties leading to flocculation, whereas electrostatic stabilization dominates at pH values far from the IP.[10,11] Ionic strength has also been shown to change the conformational arrangement of block polyampholytes and to strongly influence protein solubility, due to a charge screening effect.[12,13] Although electrostatic stabilization of zwitterionic components is easy to achieve, a drawback is the decreased charge accessibility; a desirable feature for drug delivery. In order to ensure particle stabilization while retaining their surface and charge accessibility, depletion stabilization has been previously employed to stabilize several colloidal particles, including gold[14] and silica particles.[15] This mechanism occurs when particles, in the presence of non-adsorbing polymers, gain configurational entropy over the attractive osmotic pressure caused by the depletion layer.[16] This phenomenon occurs at polymer concentrations beyond the concentration required to induce depletion flocculation due to the overlapping of the polymer, which decreases the attractive osmotic energy.[16]

Zwitterionic components, such as proteins, can compete with food supplies, whereas block polyampholytes are not necessarily biodegradable or derived from renewable sources. Here we describe a novel route for the production of plant-based zwitterionic cellulose nanofibrils (ZCNF), based on the reported TEMPO-mediated oxidation[17–19] and glycidyltrimethylammonium chloride (GTMAC) cationization reactions.[20,21] This functionalization route involves the selective introduction of negatively charged carboxyl groups[17,19,22] by oxidation followed by grafting of quaternary ammonium groups from the GTMAC-cationization.[21] Although pathways for the production of cellulose nanofibrils (CNF) bearing oppositely charged moieties have been reported,[6,7] their self-assembly in aqueous media has not, to the best of our knowledge, been reported, although the colloidal properties of oxidised cellulose nanofibrils (OCNF)[18,23–25] and quaternary ammonium salt grafted CNF[21,26,27] aqueous dispersions have been characterized. Here we describe the functionalization and double-charge nature of ZCNF revealed by ^{13}C nuclear magnetic resonance (NMR) spectroscopy and ζ-potential measurements. The relative stability and structure of dispersions of ampholytic ZCNF in aqueous media containing the anionic surfactant sodium dodecyl sulfate (SDS), cationic surfactant dodecyltrimethylammonium bromide (DTAB) and non-ionic surfactant TWEEN® 80 (TW80) was investigated via ζ-potential, transmission electron microscopy (TEM), rheology and small angle neutron scattering (SANS).

Materials and methods

[a] Department of Chemistry, University of Bath, Claverton Down, Bath, BA2 7AY, UK. E mail: k.edler@bath.ac.uk; Tel: 01225 384192
[b] School of Pharmacy, University of East Anglia, Norwich Research Park, Norwich, NR4 7TJ, UK. E mail: j.angulo@uea.ac.uk, y.khimyak@uea.ac.uk
[c] Centre for Sustainable Chemical Technology, University of Bath, Claverton Down, Bath, BA2 7AY, UK. E mail: j.l.scott@bath.ac.uk University of Bath Tel: 01225 386307Address here.

†Electronic Supplementary Information (ESI) available: Material characterisation, conductimetric titration and attenuated total reflectance Fourier transform infrared (ATR-FTIR) spectra. See DOI: 10.1039/x0xx00000x

View Article Online
DOI: 10.1039/C8SM00752G

Sample preparation

OCNF, prepared using a TEMPO/NaOCl/NaBr oxidation[28] of wood pulp followed by high-pressure homogenization, was provided by Croda® International Plc (Goole, UK) as an 8 wt% slurry. The material was purified by dialysis to ensure that any salts or other process related impurities were removed. In brief, 20 g of OCNF was suspended in 100 mL of DI, dispersed by thorough stirring at room temperature, acidified to pH 3 using 1 M HCl (aq) and dialysed (Sigma-Aldrich® cellulose dialysis tubing, molecular weight cut-off 12400 Da) against deionised water, DI, for 3 days with daily replacement of DI. The dialysed OCNF was processed via mechanical shear (ULTRA TURRAX, IKA T25 digital, 30 min at 6500 rpm) and the pH adjusted to 7 using 0.1 M NaOH (aq). After a second dialysis step (as previously reported) the dispersion was diluted to *ca* 2 wt% (dry-basis) and dispersed by sonication: Ultrasonic Processor FB-505, Fisher, 200 W·cm^{-2}, equipped with 1 cm probe, series of 1 s on/ 1 s off pulse mode for a net time of 5 mins at 60% amplitude on *ca* 45 mL dispersion contained in a ice bath. Post-purification, stable OCNF dispersions (degree of oxidation (DO) 25%, relative to the hydroxyl group in C6 of the anhydroglucose units, measured by conductometric titration, †ESI, Fig. S1, [17,21]) were prepared. The OCNF dispersion was freeze-dried and used as the substrate for the glycidyltrimethylammonium chloride (≥90 %) (GTMAC, Sigma-Aldrich®) functionalization. NaOH powder (15.7 wt% relative to OCNF dry weight), ultra-pure DI water (18 MΩ.cm, weight ratio OCNF/water = 1/23) and GTMAC (20 mol eq. relative to anhydroglucose units (AGUs) were added to the freeze-dried OCNF. The mixture was stirred for 15 h, heated in a water bath at 65 ± 1 °C for 80 min with constant stirring in a sealed vial, cooled to 25 °C and the reaction quenched by addition of EtOH. To purify the resultant ZCNF dispersion, the suspension was centrifuged (5 min at 3600 RCF) and the pellet collected and redispersed in DI water; the process was repeated 10 times. This ZCNF dispersion was, treated as the stock from which all others were prepared. ZCNF were dispersed by sonication (Ultrasonic Processor FB-505, Fisher, 200 W·cm^{-2}, equipped with 0.63 cm probe), using a series of 1 s on / 1 s off pulses for 2 min at 60% amplitude in *ca* 45 mL of suspension. The pH of the ZCNF stock dispersion was 6.8 and not adjusted except where otherwise stated. The concentration (wt%) of the ZCNF stock dispersion was determined by gravimetric analysis and specific ZCNF concentrations were obtained by dilution of the ZCNF stock dispersion with DI water. The ZCNF dispersions at various pHs were obtained by addition of 1 M HCl (aq) or 1 M NaOH (aq) and ZCNF dispersions containing surfactant were prepared by addition of previously dissolved surfactant and vortexed thoroughly.

Methods

Rheological analyses were performed using a stress-controlled rheometer (Discovery HR-3, TA instruments®) at 25°C equipped with a sandblasted plate-plate geometry (40 mm). The samples were vortexed thoroughly to ensure homogeneity before loading and pre-sheared for 30 s at a shear rate of 1 s^{-1} prior to measurement of shear viscosity (25 to 100 s^{-1}). The viscosity data are presented as relative viscosity, η_r, defined as the apparent viscosity, η_{app}, normalized by the viscosity of continuous phase, η_{cp}.

ζ-Potential measurements were conducted using a Malvern Zetasizer Nano ZSP®. The samples were diluted to 0.01 wt% ZCNF by addition of water containing HCl (aq) or NaOH (aq) to achieve a specific pH, or surfactant solution, placed in the capillary electrode cell and the ζ-potential determined as an average of 4 measurements of 100 scans each.

The shape and size of ZCNF fibrils was investigated using TEM (JEOL JEM-2100, at 200 kV operating voltage). One droplet of the sample (0.01 wt%) was placed on a hydrophilized copper grid (previously glow discharged), allowed to rest for 30 s and the excess removed using filter paper. A droplet of 2% uranyl acetate was added on top of the grid-sample substrate and the excess removed after 30 s.

The surface tension at the air water interface (γ_{aw}) was measured using the Du Noüy ring method (Sigma 701 instrument, Attension, Sweden®) using a 9.58 mm platinum ring. ZCNF dispersions at 0.001 wt% were prepared by dilution with DI water and the γ_{aw} in a vessel with diameter of 66 mm. Afterwards, an aliquot of surfactant solution was added to the dispersion (drop wise to the air-water interface) and the evolution of the γ_{wa} in the static solution was monitored for 60 min. It is noted that the surfactant concentrations (125 µM SDS,125 µM DTAB and 2.5 µM TW80) were chosen to be below the critical micelle concentration (CMC) of the surfactants.[29,30] Control samples were prepared using DI water instead of the ZCNF dispersion.

Small angle neutron scattering (SANS) data were collected on SANS2D and Larmor beamlines (Rutherford Appleton Laboratory, Didcot, UK) using wavelengths between 1.5 and 14 Å to obtain a q-range between 0.004 and 0.6 Å^{-1}. Freeze-dried ZCNF was dispersed in D_2O by sonication, as described above, and ZCNF dispersions containing surfactant were prepared by addition of deuterated surfactants, d-SDS and d-DTAB (in dry form, provided by the ISIS Deuteration Facility) and thorough vortex-mixing. Samples were loaded into 1 mm thick quartz cells. Background subtraction and normalization of the scattered intensity $I(q)$ (cm^{-1}) was conducted using the Mantid software routine and data modelling was conducted using the software Sasview 4.0.1.[31] In agreement with the particle morphology observed by TEM measurements, ZCNF were modelled as flexible cylinders with elliptical cross sections and uniform scattering length densities, based on the worm-like chain model of Kratky and Porod with the incorporation of the excluded volume effect as described by Pedersen and Schurtenberger.[32] The Kuhn length, b_{Kuhn}, (twice the persistence length) and the major radius, r_{maj}, of the cross-section were fitted variables while the fibril contour length, L_c, and minor radius, r_{min}, were fixed. The parameter L_c could not be determined within the probed q-range, therefore, it was fixed at an arbitrary value of 1000 nm, $L_c \gg (2\pi/q_{min})$ whereas r_{min} was fixed to 1 nm, based on SANS data obtained for CNF.[27]

View Article Online
DOI: 10.1039/C8SM00752G

Solid state NMR experiments were performed at room temperature using a Bruker Avance III spectrometer equipped with a 4 mm triple resonance probe operating at frequencies of 300.13 MHz (^{1}H) and 75.47 MHz (^{13}C). Quantitative 1D ^{13}C{^{1}H} direct polarization (DP) NMR experiments were conducted at MAS rate of 10 kHz for ZCNF and OCNF powders tightly packed in an 80 µL rotor (Figure 1, †ESI Fig. S3). It should be noted that to prove covalent grafting of the GTAMC to the OCNF fibrils, excluding the hypothesis of ionic complexation between the negatively charged carboxyl group and the oppositely charged ammonium group, ^{13}C DP NMR spectra were collected for the freeze-dried powder before and after being thoroughly washed with acid solution (pH 2) and dialysed against DI (Figure 1, †ESI Fig. S3). Relaxation delays of 200 (for 4 k scans) and 800 s (for 512 scans) were employed for the washed and non-washed ZCNF powder, respectively (Figure 1, †ESI Fig. S3). It should be noted that an 800 s recycle delay is sufficient for full relaxation of ^{13}C nuclei in cellulose samples.[33] All spectra were referenced with respect to TMS. The degree of cationic substitution (DS) of ZCNF was estimated using Eq. 1.[34]

$$DS = \frac{[area\ of\ the\ methyl\ carbons\ resonance\ at\ 55\ ppm]}{[3\ \times (area\ of\ C1\ resonance\ at\ 105\ ppm]} \quad (1)$$

Results and discussion

The ampholytic character of ZCNF was revealed by solid state ^{13}C NMR and ζ-potential measurements. Quantitative solid state ^{13}C NMR spectra confirmed the presence of the quaternary ammonium group on the ZCNF (peak at 55 ppm),[34] and a DS (Eq. 1) of 23% was obtained (Fig. 1). In addition, comparison of the C4 chemical environments in OCNF and ZCNF ^{13}C{^{1}H} DP NMR spectra (84 and 89 ppm for the amorphous and crystalline features, respectively[35]) showed similar intensity peaks for the crystalline and amorphous components, indicating that no significant change was caused to the crystalline structure of ZCNF upon GTMAC functionalization (†ESI Fig. S3). ^{13}C{^{1}H} DP MAS NMR spectra of both OCNF and ZCNF showed the presence of the carboxyl group carbon atom at 175 ppm (†ESI, Fig. S3).[25,36] The ^{13}C{^{1}H} DP MAS NMR spectrum acquired with 800 s relaxation delay (Figure 1), in line with previously reported estimate for the relaxation delay,[33] showed the same DS value as with 200 s (†ESI Figure S3).‡

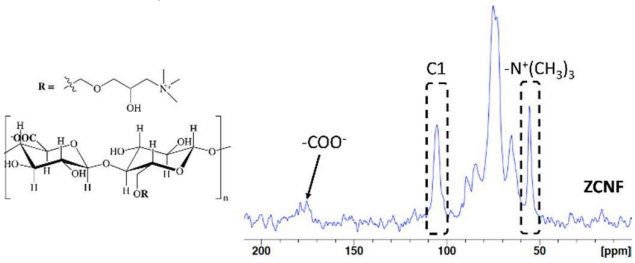

Fig. 1 ^{13}C{^{1}H} DP MAS NMR spectra for ZCNF powder (after thorough washing with acid solution (pH 2) and dialysed against DI) after 512 scans, acquired on a 300 MHz spectrometer at 10 kHz MAS rate and 800 s relaxation delay.[33] A line broadening of 80 Hz was used. The peaks corresponding to the anomeric carbon and the cationic group are highlighted within dashed rectangles.

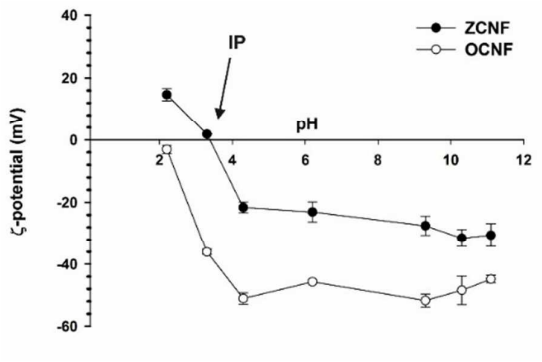

Fig. 2 The ζ-potential of ZCNF and OCNF dispersions as function of pH. The average and standard deviation of values obtained for duplicate samples are reported.

The ζ-potential of ZCNF was measured across a wide pH range, from pH 2.2 to 11.1, and further compared with that of the precursor OCNF (Fig. 2). For the pH range investigated, the ζ-potential of ZCNF is confined between +30 and -30 mV. At pH < 3.3, the ZCNF dispersions shows a positive ζ-potential, indicating that the positively charged ammonium group outweighs the charge contribution of the protonated carboxyl group. Oppositely, at pH > 3.3 the net negative ζ-potential indicates that the negatively charged carboxyl group outweighs the positively charged ammonium group. The IP of ZCNF was estimated to be between pH 3.3 and 3.5. As previously reported, the ζ-potential of OCNF remains negative over the range of pH tested, approaching neutrality at pH values close to the pKa of the carboxyl group.[37] The presence of oppositely charged moieties on the ZCNF surface strongly affected the stability of ZCNF aqueous dispersions at pH 6.8 upon addition of ionic and non-ionic surfactants.The stability of aqueous ZCNF dispersions was investigated upon addition of negatively charged SDS, positively charged DTAB and non-ionic TW80, referred to henceforth as ZCNF+SDS, ZCNF+DTAB and ZCNF+TW80 respectively. From visual observation, the 0.5 wt% ZCNF dispersions in the presence of 25 mM SDS, DTAB and TW80 showed different behaviour (Fig. 3a): 2 h after preparation, the ZCNF+DTAB dispersion shows similar turbidity to the ZCNF dispersion without surfactant, but the ZCNF+SDS exhibits decreased turbidity, suggesting a noteworthy reduction in aggregate size. Although less pronounced than the case of ZCNF+SDS, the ZCNF+TW80 dispersion also shows a decrease in turbidity, suggesting the presence of smaller ZCNF aggregates following TW80 addition. After 3 days, all the dispersions show some sedimentation (Fig. 3b). The ZCNF+DTAB and ZCNF+TW80 samples show similar sedimentation to the surfactant-free dispersion, but the ZCNF+SDS sample shows a smaller quantity of more translucent sediment. Measurement of particle surface charge

‡ *The DO of* ca. *25% was obtained for OCNF by conductometric titration; however, titration was not considered a suitable method to calculate the DO of ZCNF due to the presence of oppositely charged moieties (†ESI, Fig. S1 for conductimetric titration of OCNF and ZCNF).*

View Article Online
DOI: 10.1039/C8SM00752G

has been used to investigate the electrostatic stabilization of CNF as function of ionic strength,[23] pH,[37] and upon surfactant addition.[38] As such, the ζ-potential of ZCNF in the presence of 25 mM SDS, DTAB and TW80 was investigated (Fig. 3c).

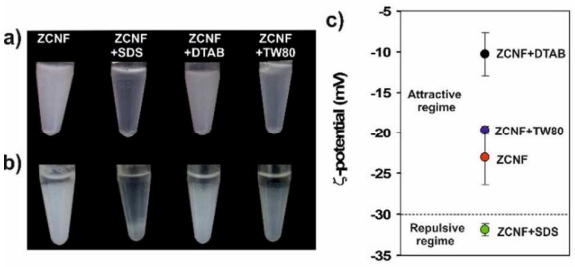

Fig. 3 Images of 0.5 wt% ZCNF dispersions upon addition of 25 mM SDS, 25 mM DTAB and 25 mM TW80 after a) 2 hours and b) 3 days after preparation. c) The ζ-potential of ZCNF dispersions at 0.01 wt% upon addition of 25 mM SDS, 25 mM DTAB and 25 mM TW80 are presented as an average of measurement on duplicate samples.

The pure ZCNF dispersion has a ζ-potential of -23 mV, reflecting the net negative surface charge of the fibrils at pH 6.8. The ZCNF+SDS dispersion has a greater net negative surface charge compared to the pure ZCNF dispersion (-32 mV), indicating neutralization of the positively charged ZCNF moieties via electrostatic screening provided by the negatively charged SDS. On the contrary, the ZCNF+DTAB dispersion shows a decrease in surface charge (-10 mV) due to screening of negatively charged ZCNF moieties by oppositely charged DTAB. Similarly Hu *et al.* reported a decrease in ζ-potential of negatively charged cellulose nanocrystals upon addition of positively charged surfactants.[39] It is noted that for values of ζ-potential between +/- 30 mV attractive forces are dominant over the repulsive electrostatic forces, leading to flocculation and/or aggregation of the particles.[40] Thus, the ζ-potential measurements of the ZCNF dispersions suggest electrostatic stabilization upon SDS addition (ζ < -30 mV) whereas a pronounced instability occurs upon DTAB addition (-30 < ζ < +30 mV). Addition of neutral TW80 to the ZCNF dispersion results in an insignificant change in surface charge (-20 mV), as expected for addition of non-ionic surfactant, but non-electrostatic driven adsorption of TW80 onto the ZCNF surface could not be excluded by ζ-potential measurements.

In order to probe non-electrostatic driven adsorption, surface tension measurements were performed. This experiment relies on the fact that the formation of a ZCNF-surfactant complex will exhibit different adsorption kinetics at the air-water interface compared to the individual components.

The γ_{aw} of the ZCNF dispersion did not deviate significantly from that of water (72 mN m^{-1} at 25°C), indicating a lack of surface active properties. Upon addition of SDS (dropwise at the air-water interface) to the ZCNF dispersion, the γ_{aw} decreases drastically due to the direct addition of the surface active component at the air-water interface, which induces a surfactant and γ_{aw} gradient (Marangoni effect).[10] Nevertheless, the concentration of surfactant distributed between air-water interface and the bulk approaches equilibrium with time, reflected in a plateau of γ_{aw} versus time (Fig. 4). The γ_{aw} of the ZCNF+SDS is significantly lower than the γ_{aw} of the pure surfactant in water. In agreement with ζ-potential measurements, this phenomenon suggests formation of ZCNF-SDS complexes, which have greater surface activity compared to the individual ZCNF and SDS. The addition of DTAB to the ZCNF dispersion also leads to a distinct reduction in γ_{aw} compared to pure DTAB in water. The γ_{aw} of the ZCNF+DTAB dispersion does not reach equilibrium within 60 min and a thin film is slowly formed at the air-water interface (insert image 4b). This observation supports the hypothesis that the adsorption of the positively charged DTAB onto the negative moieties of ZCNF occurs, neutralising charge, rendering the particles more hydrophobic and thus likely to migrate to the air-water interface. Similar phenomena have been previously reported, for example, protein-gum arabic coacervates are more effective at reducing the γ_{aw} than the single components alone.[41] Moreover, the slow change of γ_{aw} with time, for the ZCNF+DTAB dispersion, points to the presence of slowly migrating aggregates, compared to those occurring in the ZCNF+SDS dispersion, suggesting that larger aggregates are formed in this case. For the ZCNF+TW80 dispersion, the γ_{aw} lies within the standard deviation of the γ_{aw} of the pure surfactant, therefore, the hypothesis of a non-electrostatically driven adsorption of TW80 to the ZCNF can be discarded.

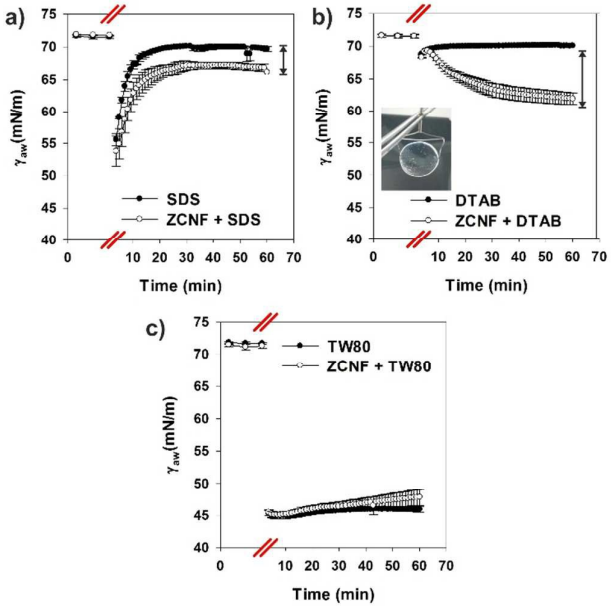

Fig. 4 Surface tension at air-water interface (γ_{aw}) of 0.001 wt% ZCNF dispersions upon addition of a) 125 µM of SDS, b) 125 µM DTAB and c) 2.5 µM of TW80. The breaks on the *x* axes indicate the addition of the surfactant to the dispersions. The average of duplicate measurements is reported. The insert in b) shows the film formed in the Du Noüy ring at the end of the experiment.

In order to gain information about shape, size and aggregation of the ZCNF, TEM images were collected (Fig. 5**Error!**

View Article Online
DOI: 10.1039/C8SM00752G

Reference source not found.). The ZCNF dispersion without surfactant shows a pronounced longitudinal fibril-fibril aggregation, resembling thick fibril-bundles with diameters up to 30 nm while the ZCNF+SDS dispersion shows individualised fibrils with a diameter of 5 nm, similar to OCNF precursor of ZCNF.[25,42,43]

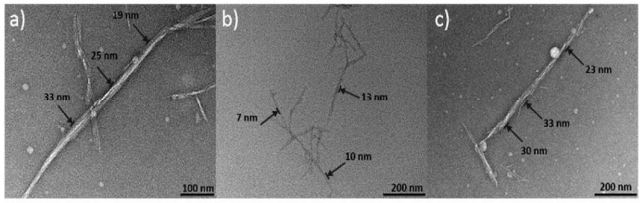

Fig. 5 TEM images of a) 0.01 wt% ZCNF dispersion, b) 0.01 wt% ZCNF with 50 mM SDS and c) 0.01 wt% ZCNF with 50 mM DTAB addition. Arrows indicate the fibril or fibril aggregate diameters (nm).

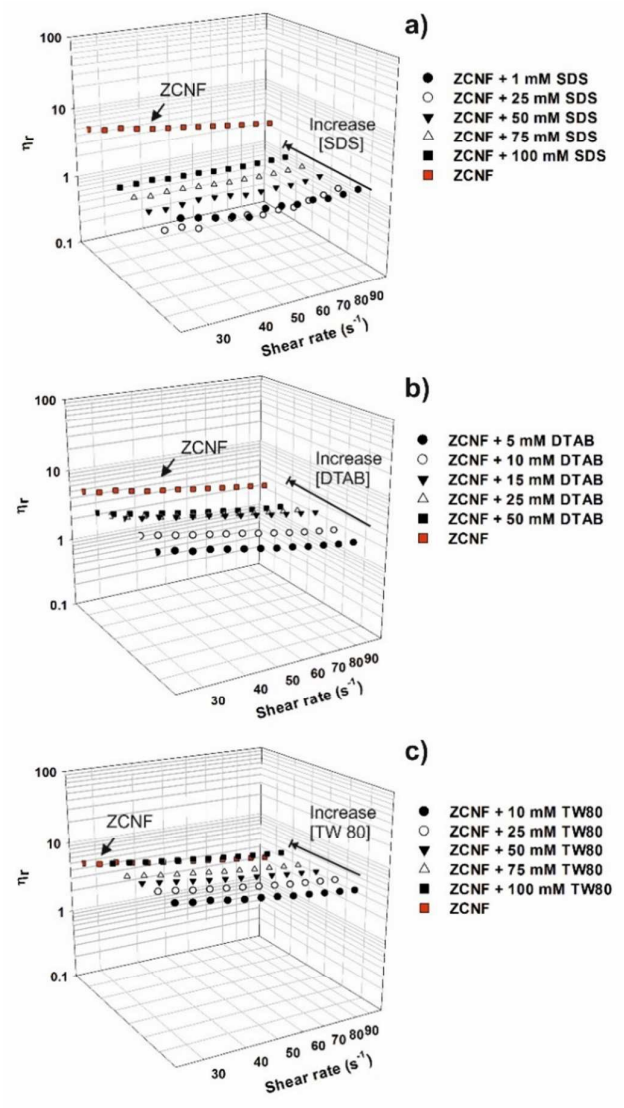

Fig. 6 Relative viscosity (η_r) as function of shear rate (s^{-1}) for 0.5 wt% ZCNF dispersions containing a) SDS, b) DTAB and c) TW80.

The presence of individualized fibrils strongly suggest that SDS leads to defibrillation of the ZCNF bundles. The ZCNF+DTAB dispersion shows thick fibril-bundles as observed for the ZCNF dispersion.

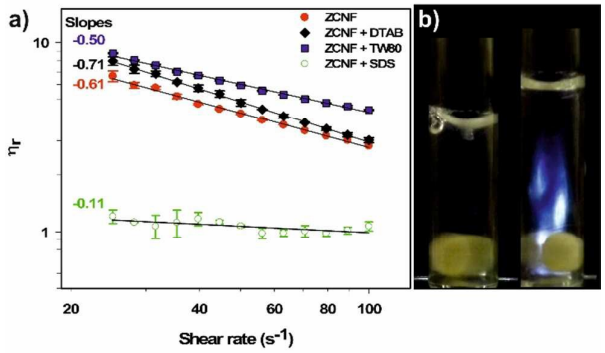

Fig. 7 a) Relative viscosity (ηr) as function of shear rate for 0.5 wt% ZCNF containing 50 mM SDS, 50 mM DTAB and 50 mM TW80. The gradients of the curves (indicated to the left of the curves) are calculated from the values of the exponent of a power law fitting (black line). b) Flow induced birefringence for a 0.5 wt% ZCNF dispersion containing 50 mM SDS (left) compared to 0.5 wt% OCNF (right). The stirred dispersions were photographed between two polarised filters

Overall, the TEM images agree with visual observation (Fig. 3) where thick fibril-bundles appear as more turbid dispersions compared to the translucent dispersions with SDS reflecting individualized and well dispersed fibrils.

In order to gain information about the evolution of the ZCNF aggregates upon surfactant addition, the shear viscosity of 0.5 wt% ZCNF dispersions was measured at different SDS, DTAB and TW80 concentrations (Fig. 6**Error! Reference source not found.**). A significant reduction in η_r occurs even upon addition of 1 mM SDS, a concentration well below the surfactant CMC (7 < CMC < 10 mM).[30] A further decrease in η_r occurs upon addition of 25 mM SDS and the values of η_r remain similar up to 100 mM SDS, indicating that only a minimal quantity of SDS, between 1 and 25 mM, is needed to achieve a significant change in rheological properties. On the contrary, the addition of different concentrations of DTAB (from 5 to 50 mM) and TW80 (from 10 to 100 mM) produce dispersions with similar rheological behaviour to the ZCNF alone dispersions.

The η_r of the 0.5 wt% ZCNF dispersions with 50 mM SDS, DTAB and TW80 were compared based on the severity of the shear thinning behaviour (Fig. 7**Error! Reference source not found.**a). A power law was fitted to the shear viscosity curves and the exponent, corresponding to the slope, used as an indicator of the shear thinning intensity ($\eta_r \sim \text{shear rate}^m$). Upon addition of SDS, the ZCNF dispersion shows a clear transition from shear thinning to an almost shear independent fluid (with a slope change from -0.61 to -0.11) alongside a noteworthy decrease in η_r. These changes in the rheological properties of the ZCNF+SDS dispersion could be assigned to *i)*

View Article Online
DOI: 10.1039/C8SM00752G

the presence of individualized fibrils and/or thinner fibril-bundles, which easily follow the direction of the flow, supporting the defibrillation suggested by analysis of TEM images (Fig. 5**Error! Reference source not found.**) or *ii)* the disruption of aggregates at shear rates below 25 s^{-1}. Conversely, the ZCNF+DTAB dispersion shows a more pronounced η_r decay upon shear (slope = - 0.71) than the ZCNF dispersion, indicating greater flocculation and the presence of aggregates that are readily disrupted by shear

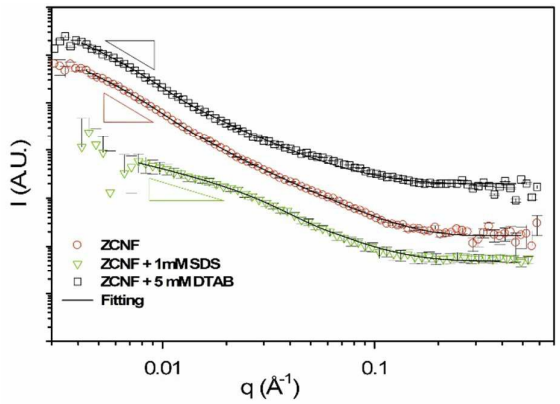

Fig. 8 SANS data for 0.5 wt% ZCNF dispersions, in the presence of 1 mM d-SDS and 5 mM d-DTAB in D_2O. The black line corresponds to a model of a flexible cylinder with an elliptical cross section used to fit the data. The Intensity (*I*) is showed in arbitrary units (A.U.). Triangles are shown to indicate the power law decay at low-*q*.

forces.[44] The ZCNF dispersion containing TW80 shows less pronounced shear thinning behaviour (slope = - 0.50), suggesting less pronounced aggregation.[44]

The weakly shear thinning behaviour of the 0.5 wt% ZCNF dispersion containing 50 mM SDS was qualitatively evaluated in terms of flow birefringence and compared to a dispersion of OCNF, the ZCNF precursor, as a positive control. Many studies have shown birefringence in cellulose dispersions and ascribed this phenomenon to the presence of nematic self-ordering of the fibrils.[18,26,42,45] The 0.5 wt% ZCNF+SDS dispersion shows no flow induced birefringence, in contrast to the OCNF dispersion. Therefore, no flow induced alignment of ZCNF occurs in presence of SDS, while a nematic self-ordering of the fibrils is observed for the OCNF dispersion as previously reported.[45]

The absence of flow induced self-ordering of the ZCNF+SDS dispersion could be ascribed to the presence of free micelles, leading to steric hindrance, as well as weak hydrophobic interactions between the surfactant tails ionically grafted onto the ZCNF surface. Similar to the ZCNF+SDS dispersion, the pure ZCNF, ZCNF+DTAB and ZCNF+TW80 dispersions exhibited no flow induced birefringence.

SANS analysis provides non-invasive sample measurements, a good statistical overview and the ability to highlight only the ZCNF structure, by contrast matching the surfactant (d-SDS, d-DTAB) to the solvent (D_2O). Thus, analysis of SANS data provided the opportunity to compare the aggregation states of ZCNF in presence of both SDS and DTAB. Data were collected for ZCNF+SDS and ZCNF+DTAB dispersions at surfactant concentrations of 1 and 5 mM respectively. These concentrations were chosen in order to match the lowest surfactant concentrations used in this study. (As d-TW80 is not readily available, contrast matching experiments (surfactant-solvent) with this surfactant were not possible.)

Table 1. Values of the parameters derived from fitting of SANS data for ZCNF and ZCNF plus d-SDS and d-DTAB, 1 and 5 mM respectively, in D_2O. Data were fitted using a model of a flexible cylinder with an elliptical cross section.

	$R_{maj\ (nm)}$	$b_{Kuhn\ (nm)}$	χ^2	D_m**
ZCNF	27.9 ± 0.4	19.4 ± 0.2	2.1	2.6 ± 0.1
ZCNF + 1mM SDS	7.51 ± 0.1	1000*	2.7	1.3 ± 0.4
ZCNF + 5mM DTAB	27.9 ± 0.5	23.8 ± 0.3	5.2	2.6 ± 0.1

*The b_{Kuhn} was fixed to the value of the L_c .

**D_m calculated in the q-range 0.005 – 0.018 Å^{-1} for ZCNF and ZCNF + 5 mM DTAB, whereas 0.008 – 0.018 Å^{-1} for ZCNF + 1 mM SDS.

None of the ZCNF dispersions, with or without surfactant, showed the presence of a Guinier region, indicating that the largest dimension of the fibril, the length, is not fully probed within the *q*-range used (Fig. 8). The minimum *q* probed is 0.005 Å^{-1}, thus, only features below 125 nm $(2\pi/q_{min})$ in size are detected in this experiment. The best data fitting, for all the dispersions, was obtained using the model of flexible cylinders with an elliptical cross section based on the wormlike micelle model.[32] In this fitting, the parameter b_{Kuhn} is descriptive of the polymer flexibility; the smaller b_{Kuhn}, the more flexible the polymer. However, for particles, such as ZCNF, this definition of b_{Kuhn} is not necessarily the most appropriate. The values of b_{Kuhn} described from fitting a semi-flexible cylinder model could suggest a convolution of parameters such as mesh size and entanglement length rather than flexibility of the fibrils. The b_{Kuhn} of the ZCNF and ZCNF+DTAB dispersions have similar values (Table 1), while for ZCNF+SDS dispersions, the b_{Kuhn} approaches a value similar to L_c (hence fixed at 1000 nm, Table 1), indicating that the fibrils behave like isolated rigid rods, further supporting the non-interacting behaviour suggested from measurements of relative viscosity. The fitting parameter associated to the elliptical cross section, r_{maj}, is in agreement with the diameters derived from measurements derived from TEM images (Fig. 5**Error! Reference source not found.**). The power law decay at low-*q* indicates the fractal-like aggregation of the ZCNF and the slope indicates the fractal dimension, D_m (Fig. 8).[46,47] The ZCNF and the ZCNF+DTAB dispersions both yield a value of D_m = 2.6 ± 0.1, indicative of dense aggregates. Similar to values derived from small angle X-ray scattering (SAXS)[48] and SANS[49] for OCNF dispersions in the absence of surfactant, the ZCNF+SDS dispersion data gives D_m = 1.3 ± 0.4, indicative of open and less dense aggregates.[47] From diffusion limited and reaction limited aggregation models (DLCA and RLCA respectively) D_m would be expected to increase with the increase of the net surface charge, due to the higher number of collisions needed to form the aggregates, until electrostatic stabilization is reached.[50] Therefore, the smaller value of D_m for ZCNF+SDS suggests that the ZCNF dispersion undergoes a transition from an unstable

View Article Online
DOI: 10.1039/C8SM00752G

to a stable regime upon SDS addition. Overall, the difference in D_m between dispersions is in agreement with previous results, where dense ZCNF aggregates show pronounced turbidity, poor stability, and severe shear thinning behaviour compared to the open and less dense aggregates formed upon SDS addition.

Conclusion

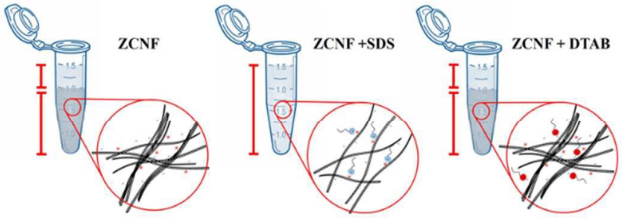

Fig. 9 Schematic of ZCNF dispersions alone and in the presence of negatively charged SDS, and positively charged DTAB.

The zwitterionic nature of ZCNF leads to the formation of fibril-bundles which further self-assemble into dense aggregates, reflected in fractal dimension D_m = 2.6, due to attractive electrostatic forces. Addition of negatively charged SDS to the ZCNF dispersion results in electrostatic complexation between SDS and the positively charged moieties present on ZCNF. The ZCNF-SDS complexes lead to electrostatically stabilized dispersions (ζ < -30 mV), leading to the individualization of fibrils which generate less turbid, more stable, lower viscosity and weakly shear thinning dispersions (Fig. 9). Upon DTAB addition, the ZCNF negative charge is partially screened due to ZCNF-DTAB complex formation leading to greater charge symmetry (ζ = -10 mV), usually associated to the formation of flocculated aggregates.[11] The more strongly flocculated nature of the DTAB containing dispersion is evidenced by the greater magnitude of shear thinning behaviour (slope of the η_r curve). Moreover, the similarity in the scattering pattern between the ZCNF and the DTAB containing dispersion indicates that the fibril-bundles assemble in a similar fashion. The addition of non-ionic TW80 to the ZCNF leads to more translucent and less shear thinning dispersions, as expected for more stable, less flocculated, dispersions.[44] Therefore, the presence of free TW80 in dispersion and the enhanced stabilization of ZCNF suggest a mechanism of depletion stabilization induced by the non-adsorbed TW80. Although still a topic of some debate, the depletion stabilization mechanism according to Fleer and Vincent occurs at polymer concentrations beyond the polymer concentration required to induce depletion flocculation and is ascribed to the gain in configurational entropy of the particles over the osmotic attractive energy caused by the depletion layer.[16,51] Nevertheless, it is noted that the concentration threshold for a change between depletion flocculation to depletion stabilization mechanism in ZCNF suspensions was not observed within the concentration range of TW80 investigated, probably due to its low CMC (12 μM).[30]

Acknowledgements

The authors thank the EPRSC for funding this project (grant numbers EP/N033310/1 and EP/N033337/1). V. Calabrese thanks the University of Bath and V. Gabrielli thanks the BBSRC for PhD studentship funding. The authors would like to thank ISIS neutron source for the award of beam time (experiment no. RB1710159) and Dr N. Mahmoudi for assistance with the experiment on beamline SANS2D. TEM images were obtained at the Microscopy and Analysis Suite in Bath University with the assistance of Ursula Potter. This work benefited from the use of the SasView application, originally developed under NSF award DMR-0520547. SasView contains code developed with funding from the European Union's Horizon 2020 research and innovation programme under the SINE2020 project, grant agreement No 654000. Data supporting this article has been made freely available via the University of Bath Research Data Archive system at DOI: 10.15125/BATH-XXXXX.

Conflict of interest

The authors declare no conflicts of interest.

References

1 V. Gold, *IUPAC Compend. Chem. Terminol.*, 2014, 1622–1622.
2 S. Kudaibergenov and A. Ciferri, *Macromol. Rapid Commun.*, 2007, **28**, 1953–1968.
3 A. Venault, W. Y. Huang, S. W. Hsiao, A. Chinnathambi, S. A. Alharbi, H. Chen, J. Zheng and Y. Chang, *Langmuir*, 2016, **32**, 4113–4124.
4 P. Liu, Q. Chen, L. Li, S. Lin and J. Shen, *J. Mater. Chem. B*, 2014, **2**, 7222–7231.
5 R. Yang, H. Jang, R. Stocker and K. K. Gleason, *Adv. Mater.*, 2014, **26**, 1711–1718.
6 T. Elschner, C. Lüdecke, D. Kalden, M. Roth, B. Löffler, K. D. Jandt and T. Heinze, *Macromol. Biosci.*, 2016, **16**, 522–534.
7 S. Liu, J. Liu, A. R. Esker and K. J. Edgar, *Biomacromolecules*, 2016, **17**, 503–513.
8 P. Trivedi, J. Trygg, T. Saloranta and P. Fardim, *Cellulose*, 2016, **23**, 1751–1761.
9 P. Zhang, F. Sun, C. Tsao, S. Liu, P. Jain, A. Sinclair, H.-C. Hung, T. Bai, K. Wu and S. Jiang, *Proc. Natl. Acad. Sci.*, 2015, **112**, 12046–12051.
10 P. Walstra, in *Physical Chemistry of Foods*, CRC Press, 2004, pp. 182–221.
11 M. A. Dyakonova, N. Stavrouli, M. T. Popescu, K. Kyriakos, I. Grillo, M. Philipp, S. Jaksch, C. Tsitsilianis and C. M. Papadakis, *Macromolecules*, 2014, **47**, 7561–7572.
12 M. A. Dyakonova, A. V. Berezkin, K. Kyriakos, S. Gkermpoura, M. T. Popescu, S. K. Filippov, P. Štěpánek, Z. Di, C. Tsitsilianis and C. M. Papadakis, *Macromolecules*,

View Article Online
DOI: 10.1039/C8SM00752G

2015, **48**, 8177–8189.
13 R. M. Kramer, V. R. Shende, N. Motl, C. N. Pace and J. M. Scholtz, *Biophys. J.*, 2012, **102**, 1907–1915.
14 X. Zhang, M. R. Servos and J. Liu, *J. Am. Chem. Soc.*, 2012, **134**, 9910–9913.
15 S. Kim, K. Hyun, J. Y. Moon, C. Clasen and K. H. Ahn, *Langmuir*, 2015, **31**, 1892–1900.
16 G. J. Fleer, J. H. M. H. Schetjens and B. Vincent, in *ACS Symposium Series, Vol. 240*, American Chemical Society, 1984, pp. 245–263.
17 D. da Silva Perez, S. Montanari and M. R. Vignon, *Biomacromolecules*, 2003, **4**, 1417–1425.
18 T. Saito, T. Uematsu, S. Kimura, T. Enomae and A. Isogai, *Soft Matter*, 2011, **7**, 8804–8809.
19 S. Tsuguyuki and A. Isogai, *Biomacromolecules*, 2004, **5**, 1983–1989.
20 J. C. Courtenay, M. A. Johns, F. Galembeck, C. Deneke, E. M. Lanzoni, C. A. Costa, J. L. Scott and R. I. Sharma, *Cellulose*, 2016, **24**, 253–267.
21 M. Zaman, H. Xiao, F. Chibante and Y. Ni, *Carbohydr. Polym.*, 2012, **89**, 163–170.
22 Y. Okita, T. Saito and A. Isogai, *Biomacromolecules*, 2010, **11**, 1696–1700.
23 H. Fukuzumi, R. Tanaka, T. Saito and A. Isogai, *Cellulose*, 2014, **21**, 1553–1559.
24 A. Isogai, T. Saito and H. Fukuzumi, *Nanoscale*, 2011, **3**, 71–85.
25 R. J. Crawford, K. J. Edler, S. Lindhoud, J. L. Scott and G. Unali, *Green Chem.*, 2012, **14**, 300–303.
26 M. Hasani, E. D. Cranston, G. Westman and D. G. Gray, *Soft Matter*, 2008, **4**, 2238–2244.
27 J. C. Courtenay, S. M. Ramalhete, W. J. Skuze, R. Soni, Y. Z. Khimyak, K. J. Edler and J. L. Scott, *Soft Matter*, 2018, **14**, 255–263.
28 T. Saito, Y. Nishiyama, J. L. Putaux, M. Vignon and A. Isogai, *Biomacromolecules*, 2006, **7**, 1687–1691.
29 M. A. Bahri, M. Hoebeke, A. Grammenos, L. Delanaye, N. Vandewalle and A. Seret, *Colloids Surfaces A Physicochem. Eng. Asp.*, 2006, **290**, 206–212.
30 D. Linke, *Chapter 34 Detergents. An Overview*, Elsevier Inc., 1st edn., 2009, vol. 463.
31 http://www.sasview.org/contact.html, .
32 J. S. Pedersen and P. Schurtenberger, *Macromolecules*, 1996, **29**, 7602–7612.
33 K. Wickholm, P. T. Larsson and T. Iversen, *Carbohydr. Res.*, 1998, **312**, 123–129.
34 H. Kono, K. Ogasawara, R. Kusumoto, K. Oshima, H. Hashimoto and Y. Shimizu, *Carbohydr. Polym.*, 2016, **152**, 170–180.
35 D. L. VanderHart and R. H. Atalla, *Macromolecules*, 1984, **17**, 1465–1472.
36 C. Tahiri and M. R. Vignon, *Cellulose*, 2000, **7**, 177–188.
37 A. B. Fall, S. B. Lindstrom, O. Sundman, L. Sundman and L. W. Odberg, *Langmuir*, 2011, **27**, 11332–11338.
38 N. Quennouz, S. M. Hashmi, H. S. Choi, J. W. Kim and C. O. Osuji, *Soft Matter*, 2015, **12**, 157–164.
39 Z. Hu, S. Ballinger, R. Pelton and E. D. Cranston, *J. Colloid Interface Sci.*, 2015, **439**, 139–148.
40 L. L. Schramm, in *Advances in chemistry*, 1996, vol. 251, pp. 21–22.
41 V. Ducel, J. Richard, Y. Popineau and F. Boury, *Biomacromolecules*, 2005, **6**, 790–796.
42 Y. Habibi, H. Chanzy and M. R. Vignon, *Cellulose*, 2006, **13**, 679–687.
43 T. Saito, S. Kimura, Y. Nishiyama and A. Isogai, *Biomacromolecules*, 2007, **8**, 2485–2491.
44 A. L. Ogden and J. A. Lewis, *Langmuir*, 1996, **7463**, 3413–3424.
45 R. K. Johnson, A. Zink-Sharp and W. G. Glasser, *Cellulose*, 2011, **18**, 1599–1609.
46 F. Cherhal, F. Cousin and I. Capron, *Langmuir*, 2015, **31**, 5596–5602.
47 B. Hammouda, in *Probing Nanoscale Structures - The SANS toolbox*, National Institute of Standards and Technology Center for Neutron Research Gaithersburg, 2010, pp. 211–225.
48 Y. Su, C. Burger, B. S. Hsiao and B. Chu, *J. Appl. Crystallogr.*, 2014, **47**, 788–798.
49 Y. Mao, K. Liu, C. Zhan, L. Geng, B. Chu and B. S. Hsiao, *J. Phys. Chem. B*, 2017, **121**, 1340–1351.
50 S. Lazzari, L. Nicoud, B. Jaquet, M. Lattuada and M. Morbidelli, *Adv. Colloid Interface Sci.*, 2016, **235**, 1–13.
51 J. Peng, a. Kroes-Nijboer, P. Venema and E. van der Linden, *Soft Matt.*, 2016, **12**, 3514.

View Article Online
DOI: 10.1039/C8SM00752G

Table of Contents Entry

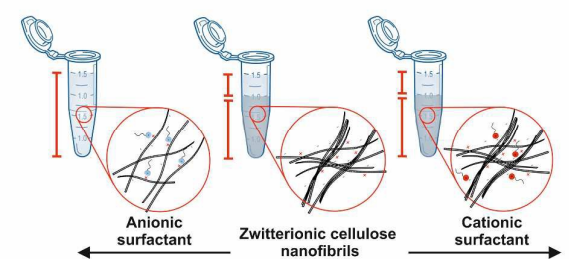

Aggregation in aqueous dispersions of zwitterionic cellulose nanofibrils can be controlled by addition of cationic and anionic surfactants.